Reprinted from G. S. Upadhyaya (ed.), *Sintered Metal–Ceramic Composites,* Elsevie
Science Publishers, Amsterdam, 1984, pp. 51–70

(4)

[13.1]

Basic Mechanisms of Liquid Phase Sintering

G. Petzow & W. A. Kaysser

Max-Planck-Institut für Metallforschung, Institut für Werkstoffwissenschaften
Heisenbergstraße 5, D-7000 Stuttgart 80, FRG

ABSTRACT

A review on the present state of liquid phase sintering in ceramic and metallic systems is given. It is shown how the densification phenomena i.e. rearrangement and center to center approach can occur by the elementary mechanisms of particle disintegration, Ostwald ripening and shade accommodation as well as directional grain growth. The influence of driving forces provided by chemical reaction on the kinetics of mass transfer is discussed.

INTRODUCTION

Liquid phase sintering is widely used for consolidation of ceramics as well . metallic powders into final shapes. Main advantages of this production methc are low sintering temperatures, fast densification and homogenization, hig final densities and resulting microstructures often providing mechanical (physical material properties superior to solid state sintered materials [1, 2 Densification during liquid phase sintering is based on rearrangement an shape change of solid constituents [3]. Chemical homogenization is fast durin liquid phase sintering due to the presence of fast diffusion paths provided b liquid phase in between the solid particles. Shrinkage and homogenization ar accelerated further by normal and abnormal grain growth. Liquid phas sintering is applied to a broad variety of systems for various purposes. Tw major types of final products may be discerned: Parts with complete or near theoretical density, fine grains and a homogeneous multiphase microstructure

and structural parts with densities in the range of 80 to 90% of TD but well predictable final dimensions, thus with low requirements for postsintering mechanical treatments. Typical materials sintered to full density are heavy metal alloys and hard metals. Typical structural parts produced for the automotive industries are made from Fe–Cu alloys. For the first type of materials shrinkage by rearrangement and shape change is of major importance, i.e., fine starting powders, high amounts of liquid phase and low green densities are used. Major purpose during liquid phase sintering of structural parts is the formation of mechanically stable contacts between the solid particles, a chemical homogenization suitable for postsintering heat treatments and the development of pore shapes which result in excellent mechanical properties.

In the subsequent review it will be shown that for both types of sintered materials a number of common basic mechanisms of liquid phase sintering exist which determine the microstructural development and final properties. Emphasis will be put on results extending previous reviews [3, 4, 5].

REARRANGEMENT

During heating up to temperature parts of the compacts form a liquid phase. Melting areas may consist of low melting particles as Ni and Fe in W heavy alloys or Cu particles in Fe based structural parts as well as of areas which have built up low melting compositions by diffusion during heating up to temperature (e.g., Fe–Ni–C). In the case of good wetting (wetting angle $\theta < 90°$) the liquid phase is pulled by capillary forces into particle necks and small pores. This liquid flow may lead to residual pores at the sites of the low melting particles if these particles were large compared to the width of particle necks or interparticle pores. Figure 1 shows a large pore (central dark spot) which has formed at the initial site of a molten Ni sphere of equal size, when liquid Ni flowed in between the fine Mo particles in the vicinity [6]. Figure 2(a) and (b) shows the microstructure of Fe–10Cu (wt%) before and after liquid phase sintering. A mixture of equal sized Fe and Cu spheres (diameter 100 μm) was heavily compacted and sintered at 1165°C for 8 min. The Cu-rich melt penetrated in between the particles at initial contact areas formed by the initial compaction and left large pores at the initial sites of the Cu-particles. The latter penetration leads to a macroscopic swelling in Fe-Cu compacts resulting from the increasing particle distances due to the additional intruded liquid phase in the contact areas [7]. In both materials capillary forces led to the movement of melt (liquid flow), whereas solid particles essentially remained at their original positons. If the network of solid particles is less rigid, capillary forces may lead to the movement of melt and to the rearrangement of particles. Rearrangement during liquid phase sintering has often been treated with the liquid bridge approach. For this approach it is assumed that liquid bridges exist between most of the adjacent particles and these bridges cause particle

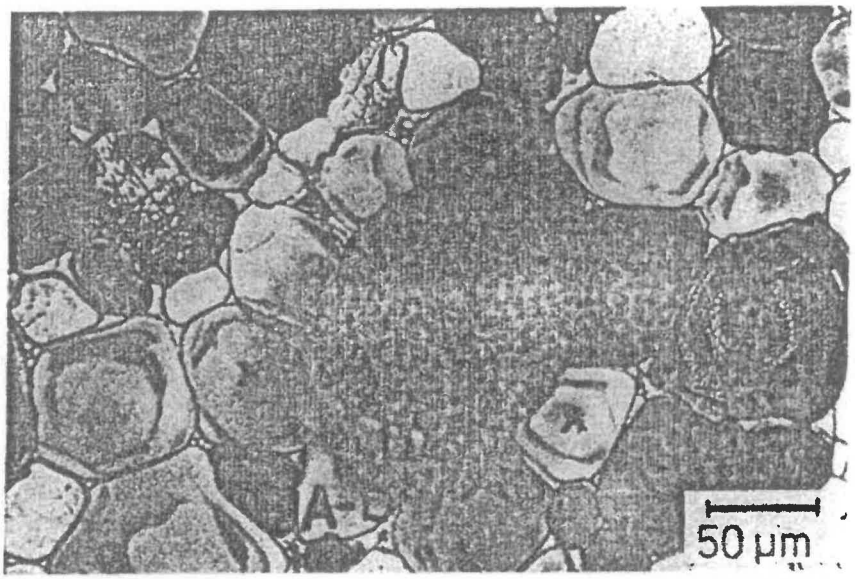

Fig. 1. 96Mo–4Ni cyclically sintered three times between 1300°C and 1460°C. Held at 1460°C for 30 min in each cycle. Microstructures around a pore obtained by strong etching (approximately 5 min) in a Murakami solution [6].

movement (rearrangement) in such a way that an overall shrinkage occurs. Since the bridges are not in contact with each other the capillary force provided by the interaction of a liquid bridge with a pair of particles is transferred to other bridges in the vicinity only by the movement of the particles. The simple basic unit of this model, two particles connected by a liquid bridge, allows the caculation of capillary forces which arise for different amounts of liquid, different particle shapes and sizes, wetting angles, and distances of particle centers [8]. Capillary forces calculated in this manner are used as an explanation for variations of the shrinkage behaviour with the parameters mentioned above. Rearrangement during liquid phase sintering has been recently observed in mono- and multilayers of Cu-coated W spheres (225 μm) and in mixtures of equal sized Cu (10 wt%) and W spheres (100 μm) [4, 9]. Figure 3 shows a volumetric mixture of tungsten and copper spheres (100 μm, 10 vol.% Cu) in a hot stages of a SEM during different stages of rearrangement. The sequence shows that, as a first step, solid particles are drawn into the liquid droplets (circles in Fig. 3(a) and 3(b)) leading to formation of clusters consisting of 5 to 20 solid particles. Due to the agglomeration of particles in liquid rich clusters, pores of different radii have been formed in the sample (circles in Figs. 3(c) to (d)). This sequence shows that the formation of liquid bridges between particles leads to rapid rearrangement and densification in small regions resulting in a porous surrounding region. The long-range shrinkage is modest. The liquid bridges between particles stabilize those porous arrays if the capillary forces created by pores are weak as in the case of large particles and low liquid contents. For large

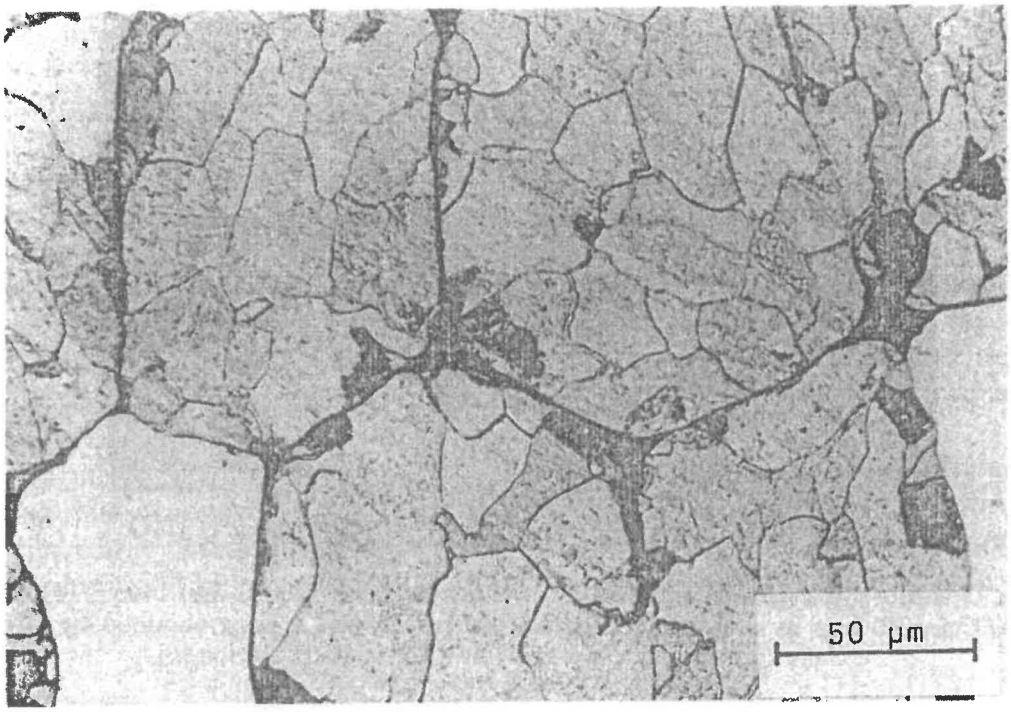

(a)

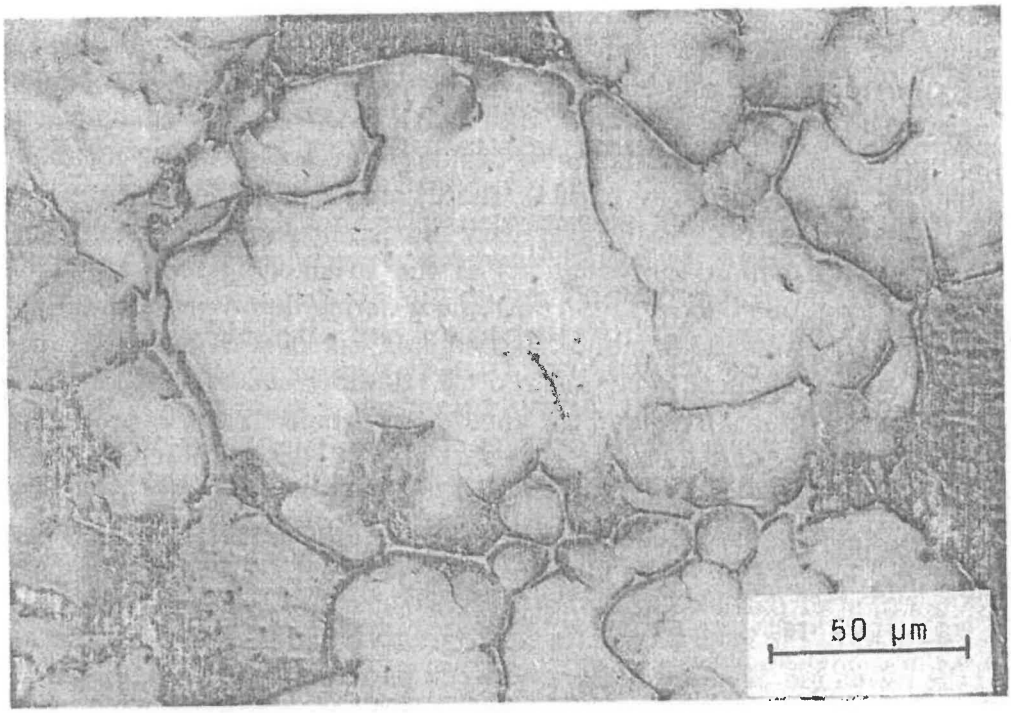

(b)

Fig. 2. Microstructure of Fe-10 wt.% Cu compacted at 785 MPa before and after liquid phase sintering [7]. (a) Before sintering; (b) sintered at 1165°C for 8 min.

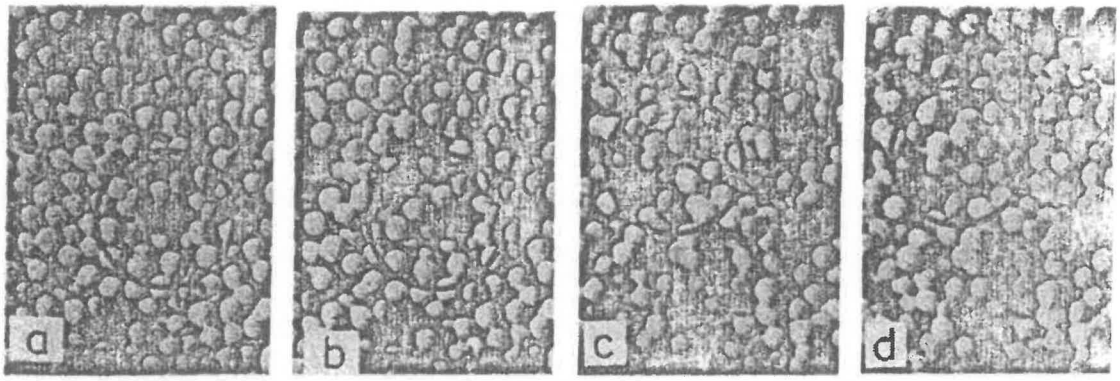

Fig. 3(a) to (d). Rearrangement of a loose-packed volumetric mixture of W spheres and 10 vol.% Cu spheres during liquid phase sintering in a hot-stage-SEM [9].

particles uniformity of packing and a high degree of mixing homogeneity are prerequisites of effective densification by rearrangement.

In systems containing particles and pores of a smaller scale or larger content of melt, pores may be eliminated by a cooperative flow of particles and liquid comparable to viscous flow of a dispersion [10]. A similar type of liquid/grain mixture flow seems to operate for the elimination of large isolated pores. Figure 4 shows three large artificial refilled pores. The pores may have formed just after melting of large Ni spheres (similar to the central pore in Fig. 1); but were refilled by liquid/grain mixture flow during liquid phase sintering for 3 min [6]. Although rearrangement in systems of small particles and high liquid contents has been a well established phenomenon for years, no analytic treatment is available at this moment.

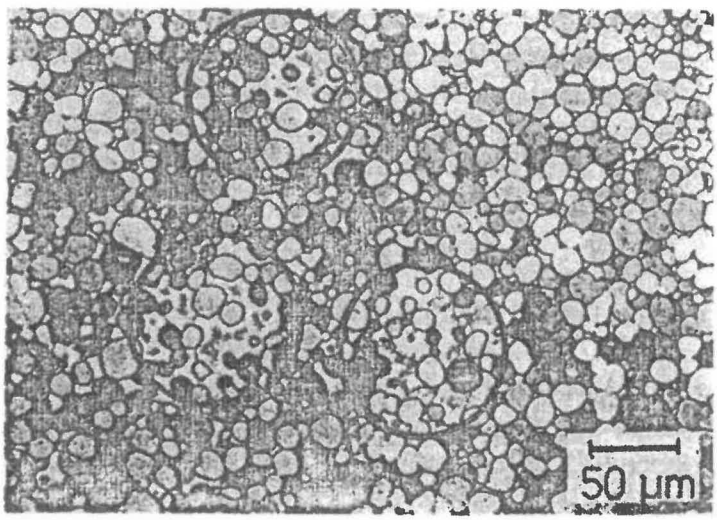

Fig. 4. Microstructure of 92Mo (7 μm)–5Ni (1·5 μm)–3Ni (100 μm) specimen sintered at 1460°C for 3 min, showing homogenized microstructure around liquid pools [6].

after liquid
min.

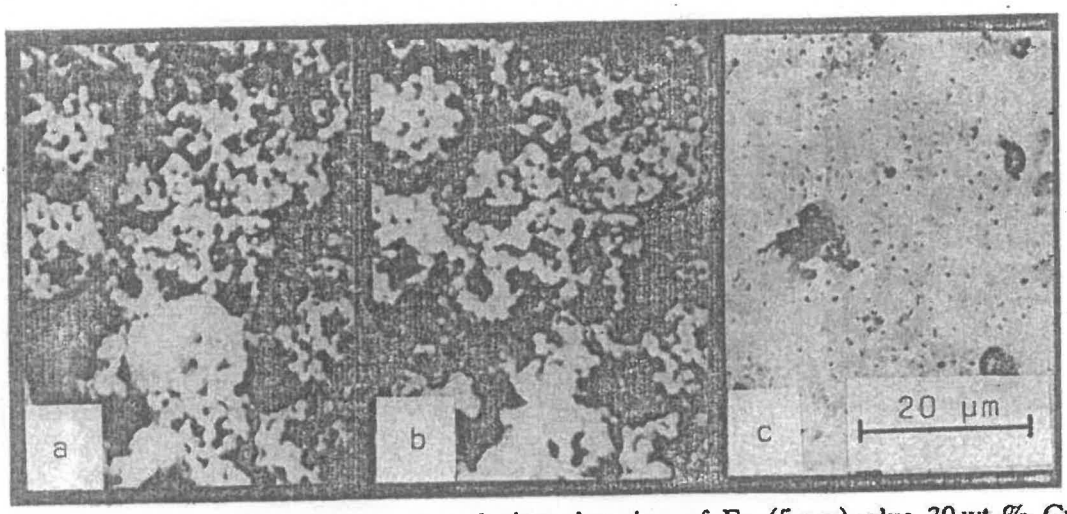

Fig. 5(a) to (c). Direct observation during sintering of Fe (5 μm) plus 30 wt.% Cu (10 μm) in a SEM with hot stage device [12].

Rearrangement of particles is a necessary requisite for effective densification throughout the sintering process, i.e. even at later sintering stages, when for example the rates of particle shape change are limiting the densification rate [11]. To discern clearly between rearrangement essentially rate controlled by the mechanical movement due to capillary forces, and rearrangement which is rate controlled by foregoing dissolution-reprecipitation processes these particle movements will be described as primary and secondary rearrangement. Important cases of secondary rearrangement result from particle disintegration, i.e. when grain boundaries are attacked and replaced by thin liquid layers. In many systems (W–Ni–Fe, Fe–Cu) a rigid skeleton of small particles forms during heating up by solid state sintering as shown in Fig. 5(a) for Fe–Cu. When Cu melts it is instantaneously drawn into small pores and necks of the Fe skeleton and essentially no shrinkage or change of particle morphology could be observed for approximately 2 min (Fig. 5(b)). This period ends with the collapse of particle chains leading to rapid shrinkage of the sample, i.e. secondary rearrangement and a surface of the specimen covered with melt [12]. Another example of secondary rearrangement is given in the chapter on particle disintegration.

SOLUTION PRECIPITATION MECHANISMS

The basic mechanisms of liquid phase sintering, which lead to a change of particle size, shape and contiguity are all connected to the dissolution of solid material in the liquid phase, transport via the melt and reprecipitation on particles at other sites. Material is dissolving at solid/liquid interfaces of higher chemical potential and reprecipitating at sites of lower chemical potential. Different chemical potentials, μ, of atoms may result from different stress

Table 1
Basic Mechanisms of Liquid Phase Sintering

Driv. force	*Mechanism*	*Densification by*	
		Rearrangement	*Shape change*
Decrease of Interfacial Energy 1–100 Jmole^{-1}	Ostwald Ripening	0	−
	Ostwald ripening with Shape Accommodation	0	+
	Contact Flattening	−	+
	Particle Disintegration	+	−
	Coalescence	0	−
	Pore Elimination by Liquid Flow	0	+
	Grain/Liquid Mixture Flow	+	0
Decrease of Free Energy <1000 Jmole^{-1}	Directional Grain Growth	0	0

Contribution to rearrangement or shape change; +, essential; 0, modest; −, negligible

states, $\Delta\mu = \Delta\sigma\Omega$, where Ω is the atomic volume or from different activities, a, of the components $\Delta\mu = kT \ln(a/a_0)$.† Stresses may e.g. be due to the curvature of solid/liquid interfaces or due to steep concentration gradients in the solid near the interface. Stresses near the interface may also result from external stresses transmitted by the melt. The latter effect is the basic physical assumption of the contact flattening theory. This theory was dominating the discussion on liquid phase sintering for two decades and often solution-reprecipitation and shrinkage were set equal to contact flattening. In recent years, however, a number of solution-precipitation mechanisms were found which seem to be of much greater importance to liquid phase sintering than contact flattening. These mechanisms are summarized in Table 1 and related qualitatively to their driving forces and their contribution to shrinkage by secondary rearrangement and shape change of the solid particles.

After prolonged liquid phase sintering of particles of 10 μm diameter the free energy of a mole of material may be lowered by 1 to 10 J due to the reduction of surface areas. Chemical homogenization or the formation of compounds during liquid phase sintering lower the energy of one mole by up to 1000 J. Thus homogenization and compound formation are expected to have considerable influence on the microstructural development, i.e. the initiation and acceleration of mass transport processes. It should be noted, however, that densification can result only as a consequence of capillary forces. The basic

† For ideal solutions and small differences $(a - a_0)$ the activities may be related to concentrations by $a/a_0 \sim c/c_0$. Then $\Delta c \sim c_0(\Delta\mu/kT) = c_0(\Delta\sigma\Omega/kT)$.

mechanisms, Ostwald ripening, particle disintegration and coalescence are caused by driving forces resulting from the reduction in solid/liquid and solid/solid interface area. Neither chemical variations nor capillary forces are required for these mechanisms. They occur in pore free liquid/solid phase systems as well. In the presence of pores (capillary forces) Ostwald ripening is connected to a shape change (shape accommodation) of the solid particles. Particle disintegration eases secondary rearrangement. Coalescence may provide some modest contribution to secondary rearrangement due to dissolving particles. Contact flattening and pore elimination by liquid flow and grain/liquid mixture flow are due only to the presence of capillary pressures. Yet all three mechanisms require solution reprecipitation of solid phase. Directional grain growth is caused by changes in the free energy of the solid constituents if material is dissolved and reprecipitated. It occurs independent of capillary forces. The latter mechanism may provide modest contribution to secondary rearrangement and shape change.

Contact Flattening

During liquid phase sinterng the initially spherical or irregular solid constituents develop a shape which is accommodated to the shape of their neighbor particles to result in a microstructure of a high density of solid phase (Fig. 1). This shape change is due to an effective pressure which arises from pores enclosed in the sintering body. If pores and the surface of the part are interconnected by liquid phase it could be rationalized that the pressure arising from inner surfaces (pores) is counterbalanced by the pressure at the outer surface if the melt is at rest [10]. The pressure from the outer surface yields compressive stresses at the contact areas of the particles. In the classical approach shape change of solid particles and shrinkage were treated as flattening of contact areas between equal sized spheres, i.e. when grain growth is absent [13]. Thin liquid films in the flat contact areas were presumed to separate the particles.† The compressive stress in the solid near the liquid films leads in binary systems to an increased concentration of solute in the melt, i.e. material will diffuse out of contact areas via the liquid films and reprecipitate elsewhere. The contact flattening approach provided simple time laws for shrinkage with $\Delta V/V_0 \propto t^{1/3}$ in systems with diffusion controlled dissolution-precipitation kinetics, which could be also read-off from experimental log–log plots of shrinkage vs sintering time [17]. Since microstructural evidences of contact flattening were rare [18] and never unambiguous, and 'correct' time laws were often measured in systems which did not fit to the basic physical assumptions of the contact flattening model, major criticism of the contact flattening approach arose in recent years [14].

Growth rate coefficients, k, measured during liquid phase sintering are usually in the order of $10^{-18}\,m^3\,s^{-1}$. Assuming a cubic time law the average

† It is still discussed whether thin liquid layers can transmit shear stresses to a considerable extent [14, 15, 16].

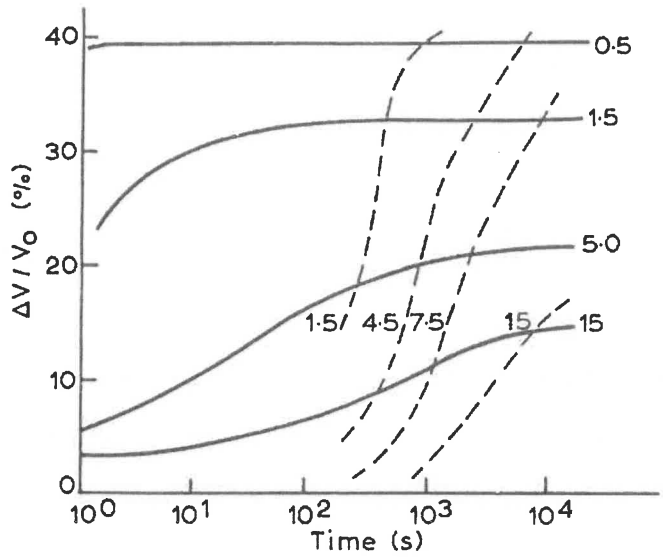

Fig. 6. Shrinkage during liquid phase sintering of Fe–20C at 1150°C. The numbers indicate the average particle radius of the initial powder. —— calculated [19], – – – measured [17].

particle radius will be doubled for the average initial radii of 0·5, 1·5, 5 and 10 μm after 0·1, 2·5, 90 and 715 s ($k = 1{\cdot}4 \times 10^{-18}\,m^3\,s^{-1}$). These short time periods indicate the importance of grain growth to all considerations upon relations between dissolution and reprecipitation and shrinkage. The classical approach treated contact flattening in the absence of grain growth. Figure 6 shows the shrinkage behavior calculated if Ostwald ripening and contact flattening are assumed to occur simultaneously [19]. The experimental results from liquid phase sintered Fe–Cu [17], where rapid grain growth had occurred by Ostwald ripening are in severe disagreement with the predicted shrinkage behavior. A similar result is obtained from analytical calculations using a particle of average size as representative of all grains yielding the shrinkage equation

$$\frac{\Delta l}{l} \sim \left\{ \frac{M}{2k} 1 - (1 + k \cdot R_0^{-3})^{-3/2} \right\}^{1/3} \tag{1}$$

where M represents some physical constants and R_0 is the initial average particle size [19]. For $k \to 0$, i.e. a system of equal sized nongrowing spheres eqn (1) reduces to the classical equation of diffusion controlled contact flattening. Grain growth slows down contact flattening and a final contact flattened shape would be obtained. The severe discrepancy between an approach taking into account grain growth and contact flattening and the experimental results, as well as the absence of unambiguous microstructural evidence of this mechanism indicate the dominant influence of other mechanisms on shrinkage during liquid phase sintering, particularly the importance of shape accommodation during Ostwald ripening.

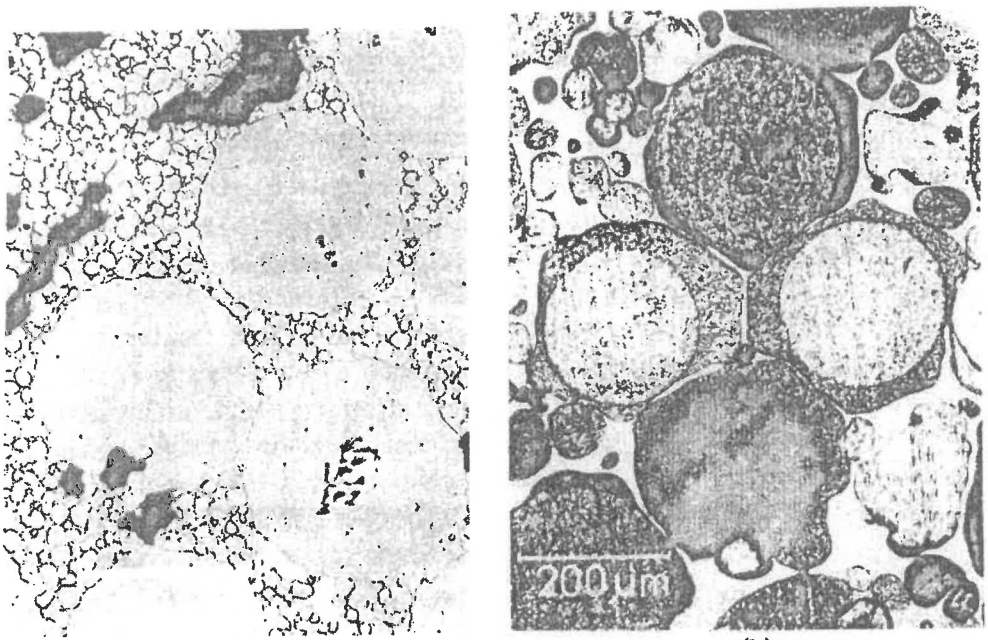

Fig. 7. Grain growth and shape accommodation during liquid phase sintering of W–Ni at 1670°C [14]. (a) 3 min; (b) 120 min.

Ostwald Ripening and Shape Accommodation

As mentioned above grain coarsening during liquid phase sintering fits reasonably well into the scheme of diffusion or interface controlled Ostwald ripening [20]. From growth experiments with a reduced non steady state particle size distribution, i.e. mixtures of small (10 μm) and large (225 μm) single crystal W powders (Fig. 7(a)) annealed in the presence of a Ni-rich melt, [14] the idea was set forth that shrinkage is directly linked to grain growth. During prolonged liquid phase sintering the small W particles partially dissolved and solid phase precipitated on to the large W spheres (Fig. 7(b)). The initial spherical shape of the large W particles changed towards polyhedral shapes (with roundish edges and corners) by the reprecipitating material, where ever large particles were in an intimate vicinity. At the same time the number and the volume fraction of small particles were decreasing due to coarsening in the set of small particles and material losses to the very large W-spheres. Simultaneously the porosity decreased from 17% after 5 min to 2% after 360 min of liquid phase sintering. Yoon and Huppmann put emphasis on the importance of a shrinkage mechanism where small dissolving particles give way to further densification by rearrangement of small and large W particles. The shape change of the large initial spheres may occur either if the spheres grow spherically during Ostwald ripening and subsequently undergo contact flattening if they come into contact with other spheres or if Ostwald ripening of the spheres occurs in a 'shape accommodating' way.

From Fig. 7(b) (arrow), it is evident that a virtual 'contact flattening' would

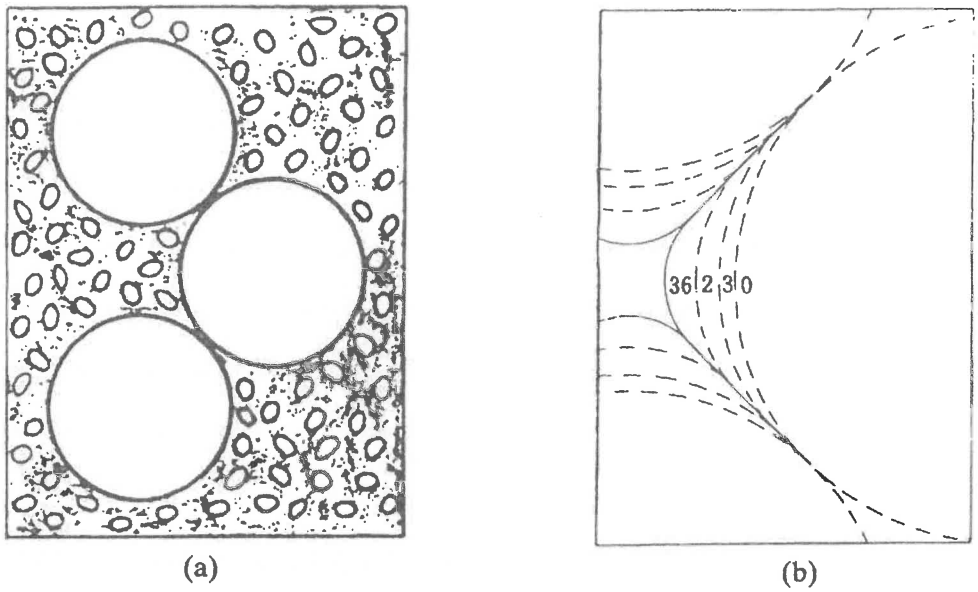

Fig. 8. Shape change of large spheres during Ostwald ripening in a mixture of small and large spheres [21]. (a) Initial state; (b) After sintering.

be a fast process which yields on spheres of a virtual diameter of 225 μm flattened areas which are 90 to 150 μm wide. Spheres which are in direct contact initially, where expected to reveal a certain contact flattening of the initial spheres, i.e. should change to partially truncated spheres. Figure 7(b) shows that the virtual contact flattening never induced the truncation of the initial spheres, although wide flat areas were found where large spheres were in intimate contact. Calculations [21] of the development of a microstructure shown in Fig. 8(a) were conducted with the assumption that the large particles take part in the usual Ostwald ripening of the arrangement. No pressure in the flat contact areas is assumed beyond a value which keeps the thickness of the thin liquid layer in the contact areas fixed at 1 μm but does not hinder mutations which result from the dissolution or deposition of additional material in the neck areas. Figure 8(b) shows the shape of the large particles (enlarged area of Fig. 8(a)) after liquid phase sintering for 0, 3, 12 and 36 min. The position of material in the contact area is extremely small, thus the distance between the particle centers remains essentially constant. This result is in accordance with the observation that some large spheres in direct contact after further liquid phase sintering show considerable shape accommodation resulting from material deposited on to the spheres (Fig. 7(b)). The effect of shape accommodation during liquid phase sintering of a liquid/solid phase system with approximately steady state, i.e. narrow particle size distribution is shown particularly well in the microstructure of Fig. 1. Many grains (indicated by a cross) develop a stronger shape accommodation during growth. Contact flattening should lead to etch boundaries joining at larger angles at least in some particles in the microstructure part of which is shown in Fig. 1, but no

evidence of this was observed [6]. In summary, shape accommodation during grain coarsening seems the main reason for shape change of solid particles during sintering. Secondary rearrangement due to the dissolution of smaller particles appears to be the dominant shrinkage mechanism.

Particle Disintegration

Attack of grain boundaries by melt is observed in many systems, e.g. Al–Ga, Cu–Bi. For liquid phase sintering the most intensive studied system is Fe–Cu [7]. Compacts of Fe spheres with 10 vol.% Cu spheres, both of 100 μm diameter (Fig. 2(a)), were sintered at 1165°C for times up to 60 min. After annealing for 3 min above the melting point of Cu, all contact regions between the Fe particles were filled with liquid. After 8 min grain boundary attack has led to severe changes in the contact area geometry; instead of the initially flat interparticle contact areas, wavy layers of liquid are present and bumps formed opposite each grain boundary consisting of Fe(Cu) solid solution (Fig. 9(a)). Figure 9(b) shows schematically grain boundary attack as a solution-reprecipitation process. Pure Fe is taken into solution at the tip of the advancing melt (B in Fig. 9(b)), transported through the liquid phase and reprecipitated as a solid solution (β) on the particle located opposite the grain boundary. This process results in removal of material from the interior of the particle and replacement with the melt. The material reprecipitation in contact areas leads to separation of particles and, in the absence of rearrangement, to macroscopic swelling [7].

Investigations of Al_2O_3-glass [22] and ZnO–Bi_2O_3 [23] systems show that penetration of the liquid is very sensitive to even small changes in the composition, e.g. the addition of a small amount of MgO to anorthite or a slight supersaturation of anorthite by Al_2O_3 (Fig. 10(a) to (c)). In addition transport kinetics are strongly accelerated with increasing solubility of the solid material in the liquid phase [22].

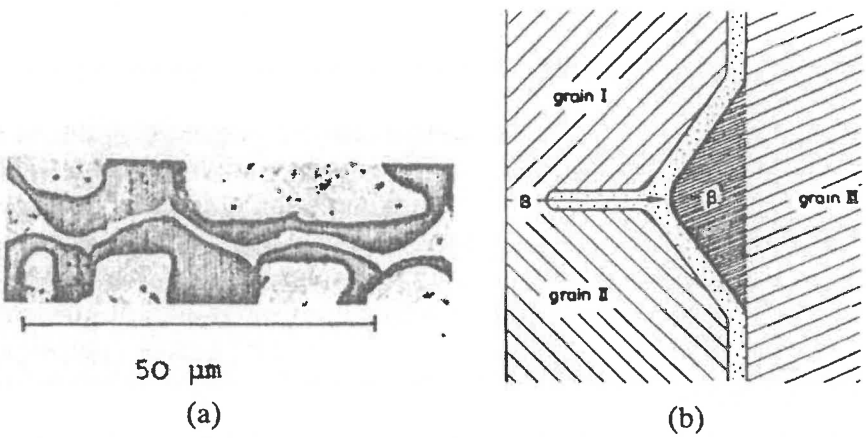

Fig. 9. Microstructure of initially flat contact area in Fe–Cu after sintering at 1165°C for 8 min. (a) Microstructure; (b) Model.

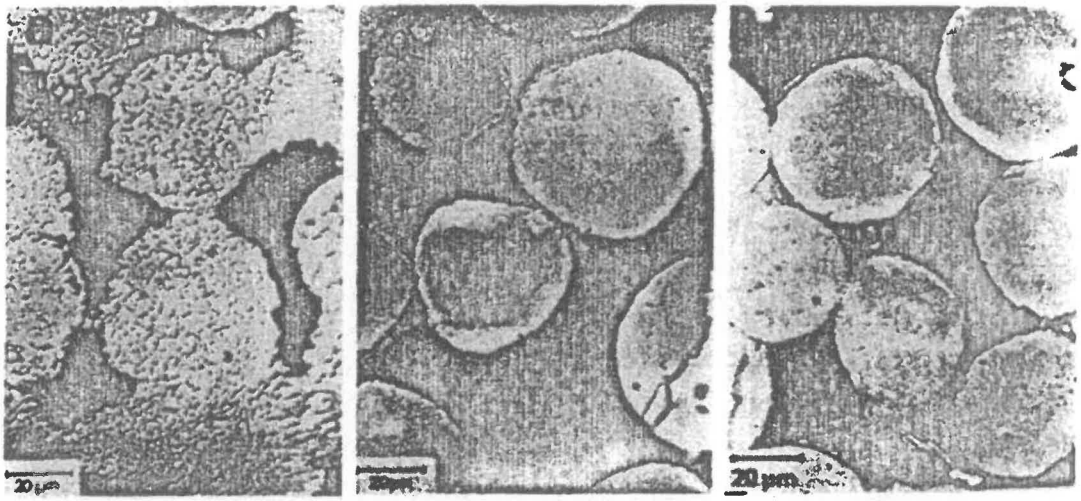

(a) (b) (c)

Fig. 10 (a). Polycrystalline Al_2O_3-spheres after liquid phase sintering at 1700°C for 1 min. Liquid phase is (a) 15 wt.% anorthite (b) 14·9 wt.% anorthite + 0·1 wt.% MgO, (c) 15 wt.% anorthite supersaturate with Al_2O_3 [4,5].

If grain boundary attack along all grain boundaries of a particle is complete, particle disintegration may occur, resulting in loss of original particle shape, as shown in Fig. 11(a) and (b) for polycrystalline Al_2O_3-spheres in a glassy phase. The disintegration of the Al_2O_3-particles leads to an increased mobility of single grains and enables secondary rearrangement and considerable shrinkage to occur.

In the Al_2O_3-glass system it was possible to separate the shrinkage due to secondary rearrangement after particle disintegration from primary rearrangement [24]. Figure 11(c) shows the dimensional change of slightly compacted Al_2O_3 glass samples sintered at different temeratures. Up to 1400°C shape and size of the polycrystalline Al_2O_3 spheres is maintained and only primary rearrangement occurs. Above this temperature grain boundary attack and particle disintegration occur and the secondary rearrangement rapidly leads to considerable additional shrinkage. Another example of particle separation by penetration of melt along grain boundaries and subsequent secondary rearrangement was described in the chapter on rearrangement.

Coalescence

Recent microstructural observations [25, 26] indicate particle coalescence as a possible mechanism of grain growth during liquid phase sintering of some systems. The coalescence mechanism was proposed to start by contact formation between particles providing low energy boundaries, neck growth and completion of the coalescence by migration of the grain boundary away from the particle neck. The formation of necks with low energy boundaries (i.e. high dihedral angles) could be shown particularly well in systems like

Fig. 11. Microstructural changes and shrinkage during liquid phase sintering of Al_2O_3-alkali borate glass [8]. (a) 1h/1400°C; (b) 1h/1700°C; (c) shrinkage; ○ after 1 min; ●, after 1 h.

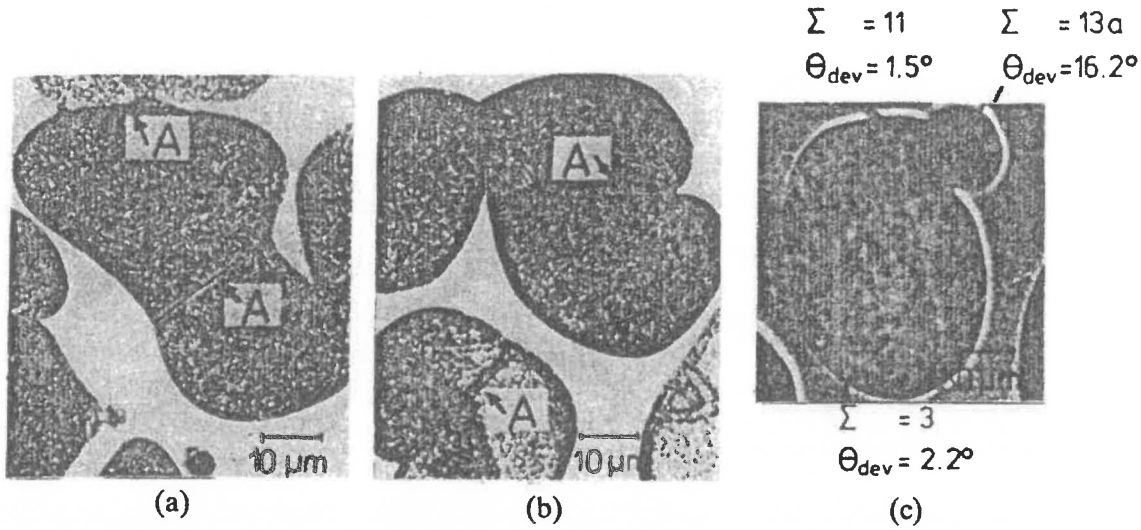

Fig. 12. Low energy boundaries after liquid phase sintering of Fe-30Cu at 1165°C for 5 h and Cu-44Ag at 800°C for 12 h [27, 29]. A indicates traces of previous austenite grains boundaries. (a and b) Fe–Cu; (c) Cu–Ag.

Fe–Cu (Fig. 12(a) and (b), [27, 28]) and Ag–Cu (Fig. 12(c), [29]). Low energy boundaries were found after liquid phase sintering of Ag–Cu between grains with small angular deviations from orientation relationships yielding Σ-values of 1, 3 and 11 [29]. A statistical treatment of grain growth by combined diffusion controlled Ostwald ripening and coalescence showed that the formation of especially large particles is likely to be caused by coalescence [27]. The contribution of coalescence to shrinkage is modest. During rapid reprecipitation at low energy necks [30], dissolution of particles in the vicinity may give rise to secondary rearrangement, but highly nonspherical particles formed by coalescence (comp. Fig. 12(a)) also may hinder particle movements.

Pore Elimination by Liquid and Liquid/Grain Mixture Flow

Shrinkage is possible by the reduction of porosity, hence the elimination of pores only. It can be shown that in the absence of entrapped gases all pores are of the surface type, which are spaces enclosed by particles which are partly covered by liquid phase. Usually the pores exert a pressure which is transmitted on to the majority of solid particles comparable to a hydrostatic external pressure. The liquid phase is under tensile stress. If the solid particles change their shape which is observed and described in the chapter on grain growth and shape accommodation, less liquid is necessary to fill up the fine capillaries between the particles than initially, thus part of the pore space can be filled with excess liquid phase. Shape accommodation may continue to complete fill up of the pore by liquid phase. This mechanism is evident for small and large pores (compared to the particle size), but easier to demonstrate for large pores (schematically shown in Fig. 13). The microstructures shown in Figs. 1 and 14 are essentially equivalent to Figs. 13(a) and (b). When

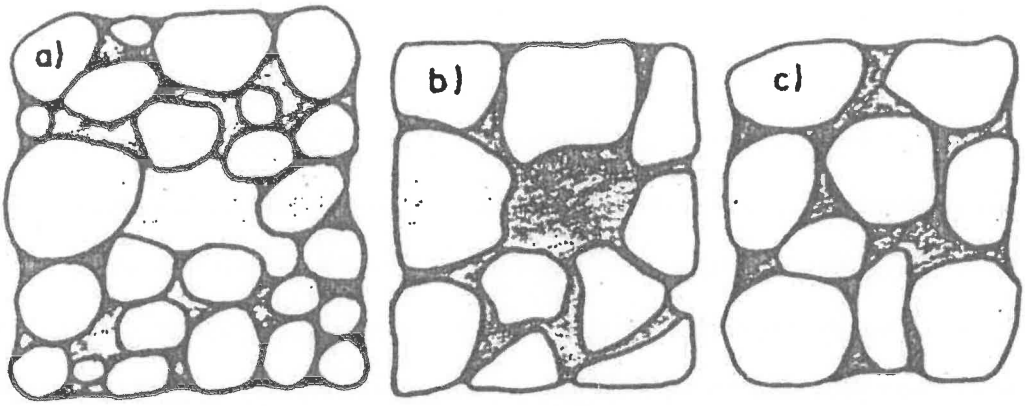

Fig. 13. Pore elimination by liquid flow. (a) Initial stage, (b) Just after filling up the pore, (c) After microstructural homogenization.

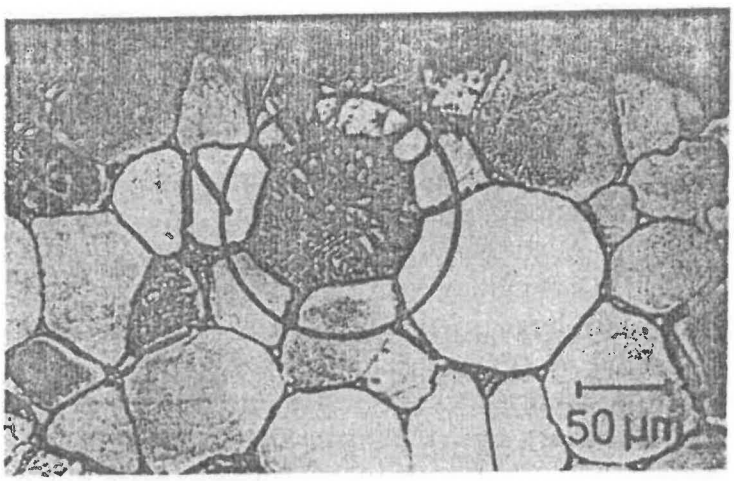

Fig. 14. Microstructure showing a liquid pool formed by liquid filling into a pore. 96Mo–4Ni cyclically sintered three times between 1300 and 1460°C. Holding times at 1460°C (60 + 30 + 30 min) [6].

the pore is filled by liquid, 'microstructural homogenization' starts by preferential precipitation of material on to concave liquid/solid interfaces facing the liquid pools.† This process continues until these interfaces have developed the same average curvature as the average interface curvature of free interfaces off the pore. In addition particles near the pore may be released from the particle set (e.g. by particle disintegration) and flow towards the liquid pool thus accelerating microstructural homogenization. Microstructural homogenization leads to a structure at the site of an initial pore which is

† Concave interfaces develop during growth of grains surrounding a pore. These grains show growth by dissolution of smaller particles and reprecipitation on larger grains along the pore. No growth is observed at Mo surfaces facing the pore's center, i.e. the growing particles follow the shape of the pore (comp. Fig. 1, [6]).

indistinguishable from other areas of the microstructure (Fig. 13(c)). The series in Fig. 13 indicates that pore elimination is equivalent to shrinkage. Due to the inhomogeneous melt distribution at that instant, the amount of melt available to fill the small interspaces between the particles is smallest and shape accommodation has to have a maximum degree. Microstructural homogenization provides an increasing amount of liquid around each particle i.e. a certain degree of respheroidization, without swelling. In real sintering bodies exists a large number of pores with a broad size distribution. As mentioned earlier small pores will be eliminated by liquid flow [31, 32]. The residual pores may become eliminated stepwise. In a many pore system with interconnected flowable liquid phase, an enclosed pore of the type shown in Fig. 13(a) is either completely unfilled or completely filled. Shape accommodation in the sintering body thus results in a precipitous complete filling of one pore and in a small temporarily increasing hydrostatic pressure in the liquid phase. The hydrostatic pressure is relaxed again by shape accommodation until another pore can be eliminated. In the absence of microstructural homogenization shape accommodation would have to develop shapes which require less and less interspace to be filled by liquid phase, i.e. solid/liquid interfaces of increasing curvature would have to develop. The increasing curvature would slow down pore elimination and would lead to a direct relation between porosity, pore size and liquid volume fraction [32]. Microstructural homogenization leads to the requirement of lower curvatures only, and lowers the driving force necessary for pore elimination. Another mechanism for pore elimination is liquid/grain mixture flow (comp. first chapter) shown in Fig. 4. It must be noted, however, that a simultaneous flow of liquid and solid particles near to the pore can only lead to a rearrangement type of shrinkage if the volume decrease in the pore area can be transmitted via solid/liquid mixture flow over long distances.

Directional Grain Growth

When single crystal W spheres of uniform size are sintered in the presence of liquid Ni, growth of one sphere at the expense of its immediate neighbour occurs (Fig. 15, [33]). This phenomenon has also been found to occur in Fe–Cu and Mo–Ni systems and is therefore believed to be a rather general process connected with the compositional difference between the pure dissolving component and the precipitating solid solution. As shown in Fig. 15(b), the microprobe analysis demonstrates that the shrinking grains consist of 100% W while the precipitated material is a W–0·15 wt% Ni solid solution [34]. This compositional difference provides a decrease in free energy of the order of $100\,\mathrm{J mol^{-1}}$ and overcompensates for the increase in interfacial energy produced by the liquid-solid area. While the growing stage is understood to be a consequence of a single solution-reprecipitation process, L. Kozma [35] and W. J. Muster [34] have shown that nucleation, which controls the growth direction, is strongly influenced by several factors. The most important ones as well as typical driving forces are summarized in Table 2. Because the

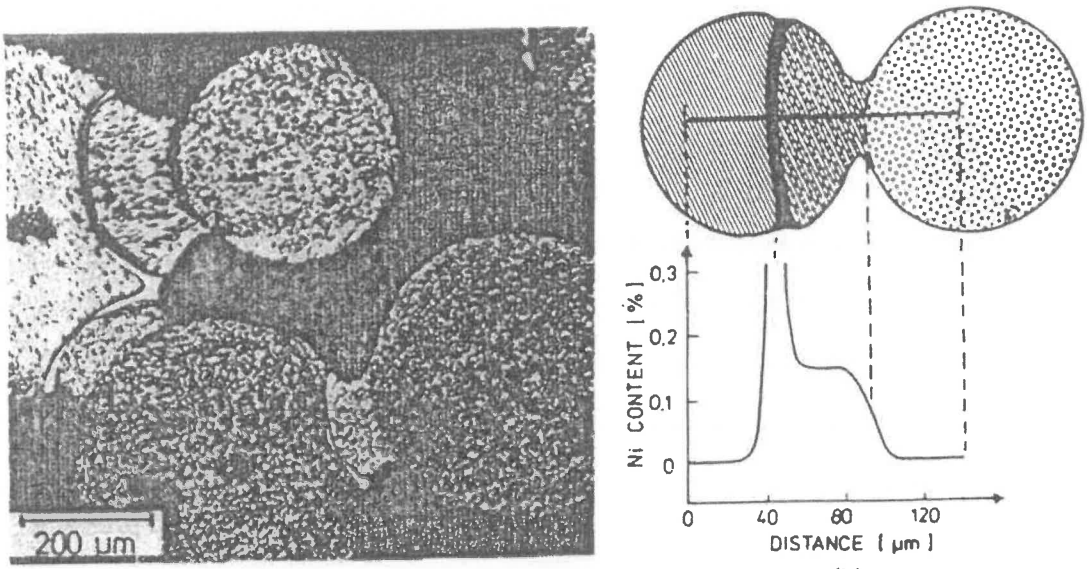

(a) (b)

Fig. 15. Directional grain growth during liquid phase sintering of single crystal W-spheres with Ni at 1670°C [33,34]. (a) Microstructure; (b) microprobe analysis.

driving forces due to temperature gradient, differences in particle size and stored energies are all of similar magnitude, small changes in the experimental conditions can determine which of these phenomena predominates the nucleation process, thus the direction of further grain growth. Because no change in grain growth direction can be expected after nucleation, the process which dominated nucleation also controls the grain growth direction. For real systems compositional differences between particles may have a dominant effect on the nucleation process, thus a dominant effect on the growth direction.

Table 2
Driving Forces for Directional Grain Growth [35]

Origin:	*Symbol*:	*Typical conditions*:	*Resulting decrease in free energy* ($Jmol^{-1}$)
Temperature Gradient	$\Delta T/\Delta x$	10°C/mm 3000°C/mm	0·086 25·00
Particle Size Difference	Δr	$r_1 = 100\ \mu m; r_2 = 70\ \mu m$ $r_1 = 100\ \mu m; r_2 = 1\ \mu m$	0·11 25·00
Internal Energy Quenched-Re-crystallized	ΔU		0·034
Free Energy of Solution (W–Ni)	ΔG		72·00

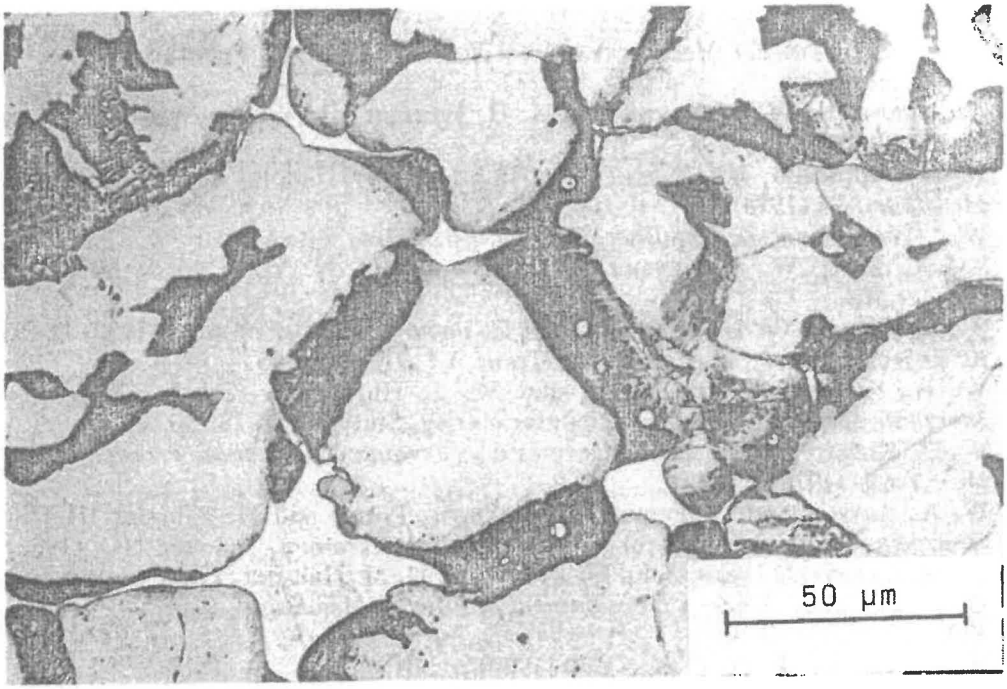

Fig. 16. Fe–10Cu–0·45C after sintering at 1150°C for 20 min.

Directional grain growth itself contributes little to densification. Shrinkage may occur similar to shrinkage due to coalescence, in connection with the filling of the negatively curved neck regions with material originating from contact regions and from small particles in the vicinity. The major importance of directional grain growth for most systems, however, is the contribution to rapid homogenization. Figure 16 shows Fe particles after short liquid phase sintering of Fe–Cu–C. The directionally grown areas are dark. In addition fast directional grain growth could be observed in Fe–Cu and Fe–Cu–C at grain boundaries penetrated by thin liquid films or at contact areas, respectively [37].

ACKNOWLEDGEMENT

Part of the described investigations were done under a joint research program between Deutsche Forschungsgemeinschaft (DFG, Pe 205/1) and Korea Science and Engineering Foundation (KOSEF). Many illuminating discussions with Prof. R. L. Coble and D. N. Yoon, Drs. S.-J. L. Kang, O. J. Kwon and J. S. Lee are acknowledged.

REFERENCES

1. W. Schatt, Pulvermetallurgie und Verbundwerkstoffe, VEB Deutscher Verlag für Grundstoffindustrie, Leipzig (1980).

2. F. V. Lenel, *Powder Metallurgy*, Metal Powder Industries Federation, Princeton, New Jersey, 1980.
3. G. Petzow and W. A. Kaysser, in H. H. Hausner (Ed.), *Science of Ceramics 10*, DKG, 10 (1980) pp. 269.
4. W. J. Huppmann, H. Riegger, W. A. Kaysser, V. Smolej and S. Pejovnik, *Z. Metallkde.*, **70** (1978) 41.
5. W. J. Huppmann, *Z. Metallkde.* **70** (1979) p. 792.
6. S.-J. L. Kang, W. A. Kaysser, G. Petzow and D. N. Yoon, to be published in *Powder Met.*
7. W. A. Kaysser, W. J. Huppmann and G. Petzow, *Powder Met.* **23** (1980) 86–91.
8. R. B. Heady and J. W. Cahn, *Met. Trans.* **1** (1970) pp. 185.
9. W. A. Kaysser, in G. Petzow and W. J. Huppmann (Eds.), *Contemporary Inorganic Materials* 1978, Dr. Riederer Verlag, Stuttgart, 1978, pp. 41.
10. W. D. Kingery, in W. D. Kingery (Ed.), *Ceramic Fabrication Processes*, Wiley, New York, (1978) pp. 131.
11. W. A. Kaysser and G. Petzow, in R. Davis, Potter and H. Palmour III (Eds.), *Emergent Process Methods for High Technology Ceramics*, Raleigh, NC, (1982).
12. W. A. Kaysser, S. Takajo and G. Petzow, in H. H. Hausner, H. W. Antes and G. D. Smith (Eds.), *Modern Development in Powder Metallurgy*, MPIF, 12 (1982) pp. 473.
13. W. D. Kingery, *J. Appl. Phys.*, **30** (1959) p. 301.
14. D. N. Yoon and W. J. Huppmann, *Acta Met.*, **27** (1979) p. 693.
15. F. F. Lange, *J. Am. Ceram. Soc.*, **65** (1982) C-23 and *J. Am. Ceram. Soc.*, **66** (1983) C-33.
16. V. Smolej, *J. Am. Cer. Soc.*, **66** (1983) C–33.
17. W. D. Kingery and M. D. Narasimhan, *J. Appl. Phys.*, **30** (1959) p. 308.
18. G. C. Kuczynski, Physics of sintering, *Journal of ITSS*, **5** (1973) p. 67.
19. W. A. Kaysser, to be published.
20. e.g. S. S. Kim and D. N. Yoon, *Acta Met.*, **31** (1983) p. 1151.
21. W. A. Kaysser, M. Zivkovic and G. Petzow, submitted to *J. Mat. Science.*
22. M. Sprißler, Ph. D. Thesis, University Stuttgart, 1982.
23. H. Lenhardt, Dipl. Thesis, University Erlangen, 1980.
24. W. J. Huppmann, H. Riegger, G. Petzow, S. Pejovnik and D. Kolar, *Science of Ceramics*, **9** (1977) 67.
25. R. Watanabe and Y. Masuda, in G. C. Kuczynski (Ed.), *Sintering and Catalysis*, Plenum Press, New York (1975) p. 389.
26. E. G. Zukas, P. S. Z. Rogers and R. S. Rogers, *Z. Metallkde.*, **67** (1976) p. 591.
27. S. Takajo, W. A. Kaysser and G. Petzow, to be printed in *Acta Met.*
28. W. A. Kaysser, S. Takajo and G. Petzow, to be printed in *Acta Met.*
29. W. A. Kaysser, S. Takajo and G. Petzow, *Z. Metallkde.*, **73** (1982) p. 579.
30. T. H. Courtney, *Met. Trans.*, **8A** (1977) p. 679.
31. W. A. Kaysser, O.-J. Kwon and G. Petzow, Proc P/M'82 Europe, Florenz (1982) pp. 23–30.
32. O.-J. Kwon and D. N. Yoon, in G. C. Kuczynski (Ed.), *Sintering Processes*, Materials Science Research 13, Plenum Press, New York, 1980, pp. 203–218.
33. D. N. Yoon and W. J. Huppmann, *Acta Met.*, **27** (1979) p. 973.
34. W. J. Muster, D. N. Yoon and W. J. Huppmann, *J. Less. Common Metals.* **65** (1979) p. 211.
35. L. Kozma, W. J. Huppmann, L. Bartha and P. Mezei, *Powder Met.*, **24** (1981) pp. 7–11.
36. W. J. Muster and H. Willerscheid, *Metallography*, **14** (1979) pp. 287–294.
37. W. A. Kaysser and G. Petzow, submitted to *Z. Metallkde.*